RMetS
Royal Meteorological Society

Austral summer foehn winds over the McMurdo dry valleys of Antarctica from Polar WRF+

Daniel F. Steinhoff,[a,b]* David H. Bromwich,[a,b] Johanna C. Speirs,[c]
Hamish A. McGowan[c] and Andrew J. Monaghan[d]

[a]*Polar Meteorology Group, Byrd Polar Research Center, The Ohio State University, Columbus, USA*
[b]*Atmospheric Sciences Program, Department of Geography, The Ohio State University, Columbus, USA*
[c]*Climate Research Group, School of Geography, Planning and Environmental Management, The University of Queensland, St Lucia, Australia*
[d]*Research Applications Laboratory, National Center for Atmospheric Research, Boulder, CO, USA*

*Correspondence to: D. F. Steinhoff, Research Applications Laboratory, National Center for Atmospheric Research, Boulder, CO, USA. E-mail: steinhof@ucar.edu

Foehn winds are a prominent feature of the McMurdo Dry Valleys (MDVs) climate, and are responsible for periods of strong winds and warming. The foehn mechanism determined from a case study presented in earlier work is shown here to be robust for a set of the MDVs summer foehn events over the 1994–2009 period using output from the Polar Weather Research and Forecasting Model (Polar WRF). Gap flow south of the MDVs is evidenced by the positive relationship between the pressure gradient and near-surface wind speed along the gap. Subsequently, mountain waves are generated and result in adiabatic warming and the downward transport of warm air into the MDVs, and differences in mountain wave characteristics depend on the ambient wind direction and the degree of flow nonlinearity. Pressure-driven channelling then brings warm foehn air downvalley.

Although a large range of synoptic-scale circulation patterns can drive foehn events, the warmest foehn events are typically associated with blocking highs over the Australian sector of the Southern Ocean, leading to warm air advection over continental Antarctica. The episodic nature of foehn events, and the tenuous connections between such events and interannual modes of climate variability, suggests that intraseasonal variability may be more important for determining their frequency and magnitude. The extraordinarily warm austral summer of 2001/2002 across Antarctica shows that advection of warm maritime air into the continental interior and strong flow aloft result in warm foehn conditions and significant melt for the MDVs.

Key Words: gap flow; blocking; intraseasonal variability

Received 8 April 2013; Revised 14 October 2013; Accepted 16 October 2013; Published online in Wiley Online Library 25 February 2014

1. Introduction

In the McMurdo Dry Valleys (MDVs), the largest ice-free region of Antarctica, winds are the controlling factor on the climate, especially the occurrence of westerly foehn winds (Speirs *et al.*, 2013). Foehn events of theMDVs are most common and strongest during winter, when valley cold pools are destroyed by foehn and air temperature can rise by up to 50 °C, with relative humidity decreasing to less than 10% (Speirs *et al.*, 2010). However, foehn events are especially important in summer, when they can cause air temperatures to rise above 0 °C and significant melt can occur, in turn supporting extensive biological activity in the soils, rocks, ephemeral steams, and glacial melt lakes (e.g. Priscu *et al.*, 1998; Fountain *et al.*, 1999). The MDVs are located between the relatively warm, maritime McMurdo Sound and the cold, dry East Antarctic Ice Sheet (Figure 1(a,b)). In addition to the ice-free valleys (Figure 1(c)), the region also features complex terrain, with mountain ranges exceeding 2000 m elevation between valleys, and the Royal Society Range (elevation upwards of 4000 m) just to the south.

Recent studies by Speirs *et al.* (2010) and Steinhoff *et al.* (2013, hereafter 'S13') show that strong westerly wind events in the MDVs are foehn, as suggested by Thompson *et al.* (1971), Riordan (1975), and Bromley (1985), and not of katabatic origin as inferred in other studies (e.g. Nylen *et al.*, 2004). Speirs *et al.* (2010) found that foehn events coincide with strong pressure gradients over the Ross Ice Shelf, typically associated with synoptic-scale cyclones

+Contribution 1436 of the Byrd Polar Research Center.

© 2013 Royal Meteorological Society

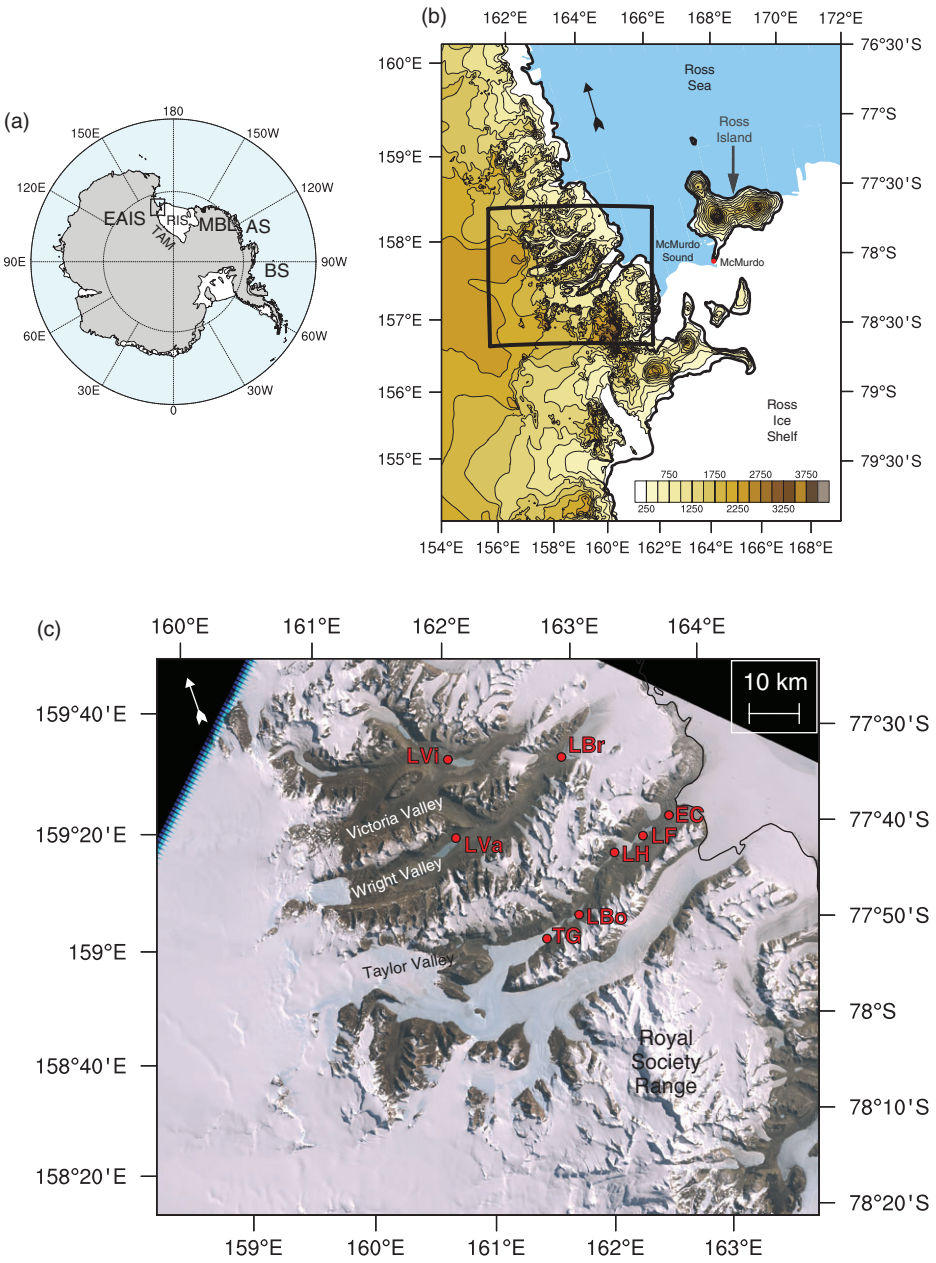

Figure 1. Overview maps of (a) Antarctica ('EAIS' is East Antarctic Ice Sheet, 'MBL' is Marie Byrd Land, 'TAM' is Transantarctic Mountains, 'RIS' is Ross Ice Shelf, 'AS' is Amundsen Sea, and 'BS' is Bellingshausen Sea) and (b) Inset of (a), the MDVs and surrounding region, with terrain height (shading, m) from RAMP data (see text). (c) Inset of (b), Landsat ETM+ image of the MDVs from 21 November 2001. Red dots indicate the LTER AWS locations referenced in this study, with abbreviations provided in Table 1. Tailed arrows in (b) and (c) point north.

off the coast of Marie Byrd Land. Steinhoff *et al.* (2013) explain components of the foehn mechanism for a summer case study, connecting the influence of the synoptic-scale circulation to strong winds and warming over the MDVs. Pressure differences along an elevated mountain gap south of the MDVs provide forcing for southerly gap flow into the western, upvalley entrance of the MDVs. Mountain waves subsequently form over the complex terrain of the elevated gap and the MDVs, leading to forced descent and adiabatic warming over lee slopes. Pressure-driven channelling then brings the warm, dry foehn air downvalley to eastern MDVs locations.

Based on the influence that the synoptic-scale circulation has on foehn-event frequency, teleconnections have been implicated to explain interannual variability in MDVs temperature and meltwater generation. Reviews of El Niño–Southern Oscillation (ENSO) teleconnections to high southern latitudes can be found in Carleton (2003), Turner (2004), and Yuan (2004). The teleconnections are manifested through Rossby wave trains (e.g. Karoly, 1989), and effects are largest in the southeast Pacific sector. Kwok and Comiso (2002) find lower (higher) sea-level pressure in the Amundsen Sea during La Niña (El Niño) events for the 1982–1998 period. However, this teleconnection is not stationary due to zonal shifts in the ENSO-related tropical convection anomalies (Bromwich *et al.*, 2004; Guo *et al.*, 2004). Cyclone density and intensity both increase (decrease) in the Bellingshausen Sea (Ross Sea) for La Niña, with opposite changes for El Niño (Pezza *et al.*, 2008). The Southern Annular Mode (SAM), or Antarctic Oscillation (AAO), is the dominant mode of atmospheric circulation variability in the southern high latitudes (Thompson and Wallace, 2000). The SAM manifests itself as zonal pressure/height anomalies having opposing signs in the midlatitudes and high-latitudes, with the positive phase implying high pressure over midlatitudes and lower pressure over high latitudes. Whereas the SAM itself influences Antarctic temperature and coastal cyclone activity (e.g. Thompson and Wallace, 2000; Pezza *et al.*, 2008), the SAM and ENSO interact to have an impact on high-latitude teleconnections (Carvalho *et al.*, 2005; Fogt and Bromwich, 2006; L'Heureux and Thompson, 2006; Gregory and Noone, 2008; Gong *et al.*, 2010; Fogt *et al.*, 2011; Ding *et al.*, 2012).

Bertler *et al.* (2004) attribute the 1986–2000 MDVs cooling trend (Doran *et al.*, 2002) to ENSO variability and the associated

© 2013 Royal Meteorological Society

shift in airmass source regions. Bertler *et al.* (2006) found phase-dependent relationships of both ENSO and SAM with MDVs summer temperatures. Using a 20 year MDVs observational climatology, Speirs *et al.* (2013) found statistically significant correlations between SAM and austral summer and autumn foehn occurrence, and between ENSO and winter temperature. Still, these connections are not robust annually and questions remain as to the role of intraseasonal variability, which is known to influence the Southern Hemisphere storm track and conditions over Antarctica (e.g. Kiladis and Mo, 1998; Kidson, 1999; Frederiksen and Zheng, 2007; Pohl *et al.*, 2010; Yu *et al.*, 2011).

Here we will first show that the foehn mechanism described in the case study of S13 is robust across a set of the MDVs foehn events spanning the 1994–2009 period. Second, we will show that blocking events over the southwest Pacific are associated with the warmest MDVs foehn events, including an example from the extraordinarily warm 2001/2002 austral summer.

2. Model, data and methods

2.1. Polar WRF

The Advanced Research Weather Research and Forecasting model (WRF-ARW, Skamarock *et al.*, 2008) Version 3.2.1 is run for austral summer (1 November to 1 March) 1994–2009. For computational efficiency, simulations are reinitialized only on the 1st and 16th days of each month, with 12 h spin-up time. To keep the synoptic-scale circulation fields in line with reality for these long simulations, four-dimensional data assimilation (FDDA or 'nudging'; Stauffer and Seaman, 1994) is used on temperature and wind fields of the top 27 vertical levels of the outermost domain only, every 6 h. Modifications for polar environments, termed Polar WRF, that were developed by the Polar Meteorology Group at the Byrd Polar Research Center, The Ohio State University (Hines and Bromwich, 2008; Bromwich *et al.*, 2009; Hines *et al.*, 2011; Bromwich *et al.*, 2013; S13) are used here. These modifications primarily encompass the land-surface model and sea ice.

A 32-8-2 km nesting structure is used for the model domains (Figure 2(a)), covering all of Antarctica and surrounding ocean in the 32 km domain, down to the MDVs region only for the 2 km domain (Figure 2(b)). Forty vertical levels are used, with the lowest level approximately 13.4 m above the surface. The model top is set at 50 hPa and all nested domains are one-way coupled. Details regarding parameterization schemes used for the simulations can be found in S13.

Initial conditions for the atmosphere, some surface fields, lateral boundary conditions, and FDDA input for the 32 km domain are supplied by the ECMWF ERA-Interim reanalysis (Dee *et al.*, 2011), provided by the Data Support Section at the National Center for Atmospheric Research (NCAR) on a regular 512 × 256 N128 Gaussian grid. Sea-surface temperature (SST) data are supplied for all domains from daily optimally interpolated Advanced Very-high Resolution Radiometer (AVHRR) and Advanced Microwave Scanning Radiometer – Earth Observing System (AMSR-E) output at 0.25° grid spacing (Reynolds *et al.*, 2007). For sea-ice concentration on all domains, we use two different datasets. The Bootstrap sea-ice concentration algorithm, used with measurements from the Special Sensor Microwave/Imager (SSM/I) instrument aboard the DMSP-F8, -F11 and -F13 satellites (Comiso, 1999), is utilized for the 1994–2007 period. Version 2 data, on a polar stereographic grid at 25 km grid spacing, were obtained from the National Snow and Ice Data Center (NSIDC). Bootstrap sea-ice data were not available past 2007, so AMSR-E output processed according to Spreen *et al.* (2008) from Universität Bremen at 6.25 km grid spacing was used for 2008 and 2009. For sea-ice thickness and snow thickness on top of sea ice, we use static climatological values from the Antarctic Sea-ice Processes and Climate program (ASPeCt, Worby *et al.*, 2008). Lateral boundary conditions, SST, and sea-ice concentration are updated for all domains every 6 h. Terrain height is interpolated from the RADARSAT-1 Antarctic Mapping Project (RAMP) digital elevation model at 200 m grid spacing (Liu *et al.*, 2001). This field is smoothed twice for all domains using a smoother–desmoother algorithm included in the Polar WRF preprocessing package. A special bare-ground land-use dataset for the MDVs is used, interpolated from 9" US Geological Service GeoTiff files provided by Kevin Manning of NCAR.

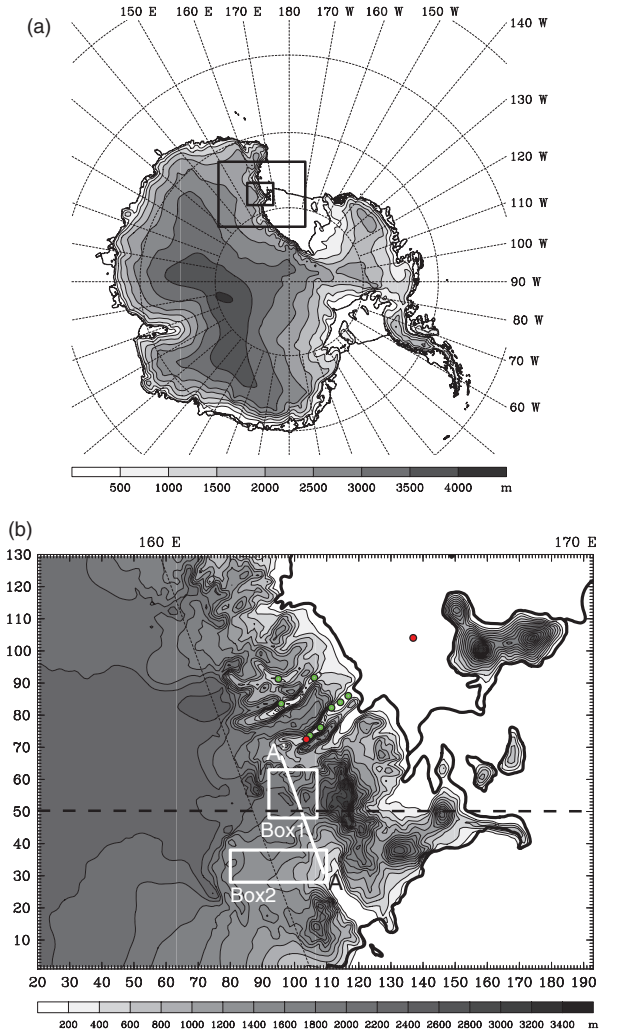

Figure 2. (a) The 32 km Polar WRF domain and terrain height (m, shaded). Solid-outlined boxes show 8 and 2 km domains. (b) The 2 km Polar WRF domain and terrain height (m, shaded). Tick marks on both axes represent model grid points. Green dots show the LTER AWS locations used in this study (Fig. 1; Table 1). Cross-section AA' and Box 1 are used in Figure 5, Box 2 is used in Figure 6, and red dots are used in Figure 7. Black dashed line at $y = 50$ is used in averaging in Figures 5 and 6.

Further modifications are made specifically for the MDVs environment, primarily encompassing land surface variables in the Noah land surface model (Chen and Dudhia, 2001). Any snow-cover input from ERA-Interim over bare ground points is removed before model initialization because the MDVs are known to be snow-free nearly perennially (Fountain *et al.*, 2010). Furthermore, we restrict Polar WRF-simulated water-equivalent snow depth over bare ground to 0.2 cm, as Polar WRF cannot simulate the removal of snow by strong foehn winds. We specify bare ground as 'loamy sand', consisting of 82% sand, 12% silt and 6% clay (Campbell *et al.*, 1998; Northcott *et al.*, 2009). Roughness length is set to 0.005 m for all bare ground points (Lancaster, 2004), and the base (no snow) albedo for the barren ground category is set to 0.18 (Thompson *et al.*, 1971; Campbell *et al.*, 1998; Hunt *et al.*, 2010). To initialize land-surface variables, Polar WRF simulations were run for one year (1 November 2005 to 31 October 2006), and the resulting 'spun up' soil fields at the end

© 2013 Royal Meteorological Society

Table 1. Murdoch Dry Valleys LTER AWS locations.

Station	Abbreviation	Valley	Latitude (°N)	Longitude (°E)	Elevation (m)
Explorers Cove	EC	Taylor	−77°35′19″	163°25′3″	26
Lake Fryxell	LF	Taylor	−77°36′39″	163°10′11″	19
Lake Hoare	LH	Taylor	−77°37′31″	162°54′1″	78
Lake Bonney	LBo	Taylor	−77°42′52″	162°27′51″	64
Taylor Glacier	TG	Taylor	−77°44′25″	162°7′42″	334
Lake Brownworth	LBr	Wright	−77°26′1″	162°42′13″	279
Lake Vanda	LVa	Wright	−77°31′0″	161°40′4″	296
Lake Vida	LVi	Victoria	−77°22′40″	161°48′2″	351

of this simulation were used as input for simulations beginning 1 November of all years. Land surface variables are carried over to each reinitialization of the atmospheric model.

2.2. *The LTER observations*

The MDVs Long Term Ecological Research (LTER) automatic weather station (AWS) data (Doran *et al.*, 1995) are used to validate Polar WRF simulations, and AWS locations used in this study are indicated in Figure 1(c) and Table 1. Observations are at 3 m height, and relative humidity is calculated with respect to ice when air temperature is below freezing. To facilitate comparison, selected variables are output at 3 m height in Polar WRF by adjusting the height that exchange coefficients are calculated at in the surface-layer scheme. The sampling interval for observations varies with time and between sites, but since January 1998 all sites sample wind at 4 s intervals and all other variables at 30 s intervals except for Lake Bonney, which samples wind at 1 s intervals. All variables are then averaged at 15 min intervals and quality-controlled by the LTER investigators and the authors.

Care is taken to choose proper Polar WRF 2 km domain grid points for representing the LTER AWS locations (to avoid so-called 'representativeness errors', Jiménez and Dudhia, 2012). Instead of interpolating to the exact observation location from the four grid points surrounding the true LTER AWS location, the chosen gridpoint is the closest to the observation location that has the correct surface type (snow-free) and properly located within the valley geometry. All Polar WRF station points are located within 2 km distance and 100 m elevation of the actual station.

2.3. *Foehn identification scheme*

The foehn event identification scheme is based on Speirs *et al.* (2010). Using observations at 15 min frequency, *all* of the following must occur over any given six-hourly period.

- Temperature: increase of 1 °C over a 1 h period OR any reading above 0 °C.
- Relative humidity (RH): decrease of 5% over a 1 h period OR any reading below 30%.
- Wind speed: greater than 5 m s^{-1} for at least 80% of the observations, using the 15 min maximum wind speed.
- Wind direction: between 180° (southerly) and 315° (northwesterly; 360° (northerly) for Lake Vida) for at least 80% of the observations.

The 0 °C and 30% RH thresholds are justified as neither are met in the absence of foehn conditions, due to sea-breeze, valley wind, and glacier wind effects. For Polar WRF output, which is also at 15 min frequency, the criteria are adjusted to the following to compensate for model biases.

- Temperature: increase of 1 °C over a 2.5 h period OR any reading above 0 °C.
- Relative humidity: decrease of 5% over a 2.5 h period OR any reading below 30%.
- Wind speed: greater than 3.5 m s^{-1} for at least 80% of the observations

The wind direction criteria are the same. The longer time periods for the temperature and RH changes allow for slower developing foehn onset in the model, which probably results from the coarse representation of topographic effects, as similar biases in foehn development were found with the fifth version 3.3 km Polar Penn State/NCAR Mesoscale Model (Polar MM5) simulations in Speirs *et al.* (2010), but not in the 0.5 km Polar WRF simulations in S13. The reduced wind-speed threshold accounts for the use of maximum wind speed in the observations, which is not available in Polar WRF output.

Each foehn event is placed into a 6 h bin, centred on 0, 6, 12 and 18 New Zealand Daylight Time (NZDT, UTC+13 h). Only one event in the 6 h bin is required for declaration of a 'foehn event'. Note that this differs slightly from the 'foehn day' entity used in Speirs *et al.* (2010), where foehn events were placed into daily intervals, in order to better sample the evolving conditions during foehn events, which can change drastically over the course of a day (S13).

3. Foehn validation

Polar WRF foehn event validation is done over 15 summer seasons (1 November to 1 March, 1994/1995 to 2008/2009). To obtain a general idea of model performance, we compare Polar WRF distributions of foehn events occurring at two or more sites with the LTER observations. During the validation period, 740 matches are found (events in both Polar WRF and the LTER observations), 239 events are found only in the LTER observations, and 1034 events are found only in Polar WRF. Although Polar WRF identifies a majority (76%) of real foehn events, too many of the simulated events (58%) are not in the observations.

A validation analysis is now done across individual observing sites, in order to determine model performance by location over the MDVs. Figure 3 shows the interannual variability of foehn events for each individual observing site and aggregated for all stations. Polar WRF generally simulates too many foehn events across all sites, but reasonably captures interannual variability in the observed foehn event counts, as indicated by the correlation of the LTER and Polar WRF year-to-year foehn event counts above 0.9 at five of eight sites, above 0.8 at seven of eight sites, and 0.95 for all stations. Relative maxima of foehn frequency in Polar WRF that do not occur in the observations include 1999 (Taylor Glacier, Lake Hoare, Lake Fryxell, Explorers Cove, Lake Brownworth), 2005 (Taylor Glacier and Lake Bonney) and 2007 (Lake Hoare, Lake Brownworth). The decrease of foehn events from west to east is well-captured by Polar WRF. There is a diurnal cycle of foehn initiation, with 18% of events at Lake Hoare initiating 0600 local time, 40% from 0006–to 1200, 29% from 1200–to 1800 and 13% 1800. Similar distributions are found at Lake Fryxell and Lake Vanda. McKendry and Lewthwaite (1992) found that the opposing easterly sea breeze is most common during evening, and westerly winds most common during morning hours, in agreement with the results presented here. Polar WRF correctly captures this diurnal cycle, with a distribution of 11, 43, 31 and 15%, respective to the 6 h time periods listed above.

© 2013 Royal Meteorological Society

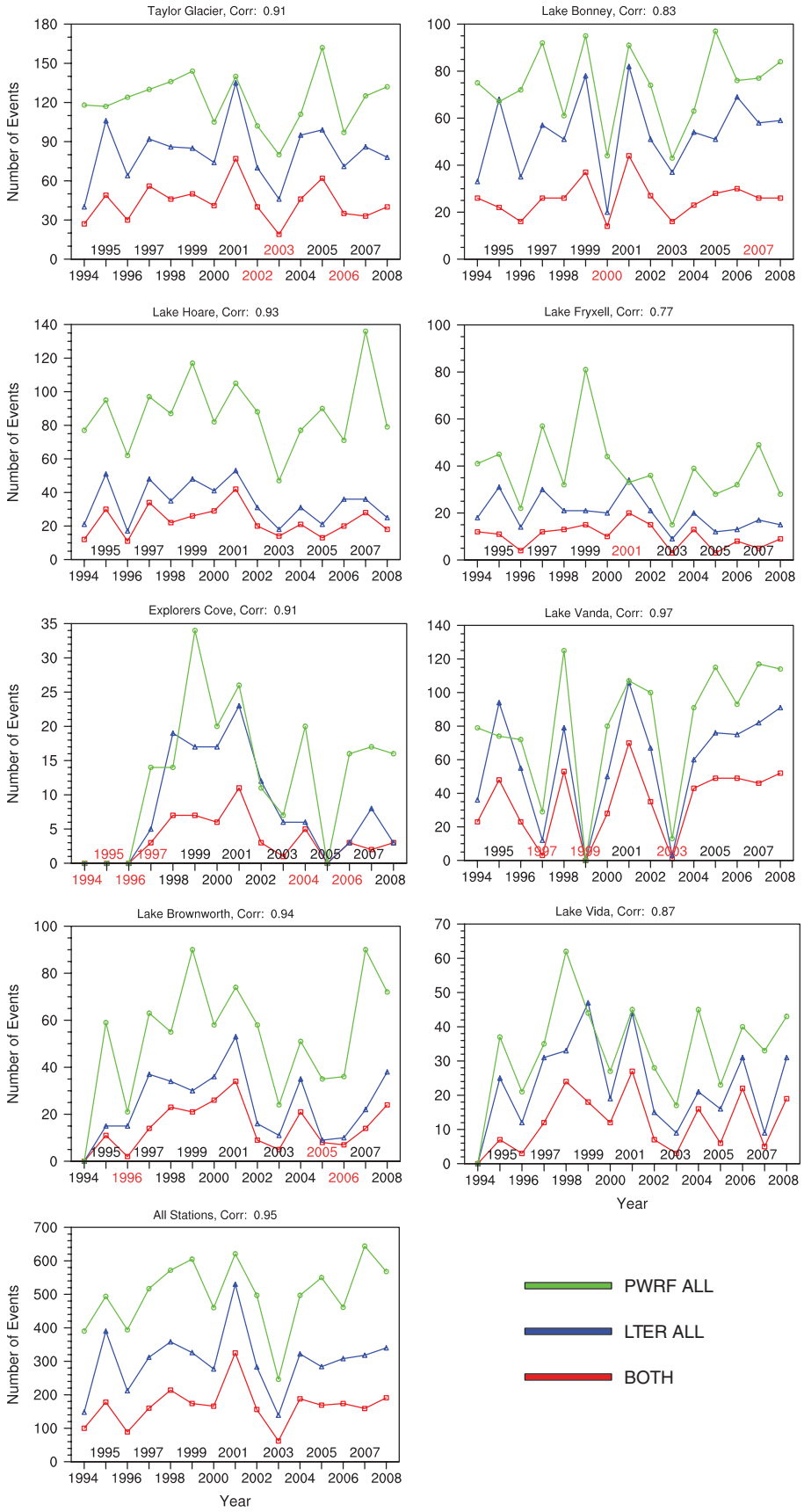

Figure 3. Interannual variability of foehn events at the LTER AWS sites for all foehn events identified in Polar WRF ('PWRF ALL', green), all foehn events identified in observations ('LTER ALL', blue), and matched events in both Polar WRF and the LTER observations ('BOTH', red). 'Corr' refers to correlation between LTER ALL and BOTH. Red-labelled years refer to years with greater than 10% missing data.

Next, we look to why Polar WRF misses some observed events, and why it generally has too many events. Figure 4(a) shows the total number of additional instances of a particular criterion that would be necessary for the number of foehn events in the observations to match the number of events in Polar WRF. Note that the values in Figure 4 are dependent on the total number of events at each site. Across all sites, wind speed and wind direction are the primary culprits. For a more detailed look at why there are too many events in Polar WRF, Table 2 shows the average number of Polar WRF events per summer ('PWRF ALL') and the average number of extra events and the percentage of the total ('PWRF EXTRA') at each site. Generally, Polar WRF has 60–70%

© 2013 Royal Meteorological Society

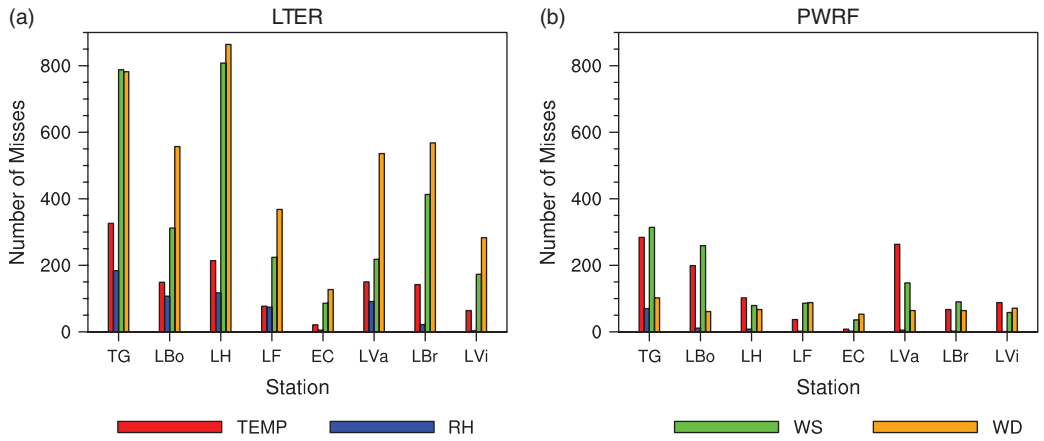

Figure 4. Number of missed criteria for foehn events at each LTER site for (a) events in Polar WRF not in the LTER and (b) events in the LTER not in Polar WRF. The LTER site abbreviations are defined in Table 1. 'TEMP' is temperature, 'RH' is relative humidity, 'WS' is wind speed, and 'WD' is wind direction.

Table 2. Extra foehn events in Polar WRF compared with the LTER observations. 'PWRF ALL' is the average number of foehn events in Polar WRF each summer; 'PWRF EXTRA' is the average number of foehn events in Polar WRF not found in the LTER observations each summer (and percentage of 'PWRF ALL'); 'PWRF STRONG', 'PWRF EXTEND', and 'PWRF OTHER' are average number of occurrences of model biases each summer (described in text); and 'PWRF NEW' is the average number of missed events each summer when discrepancies in previous three columns and their overlap are accounted for (and percentage of 'PWRF ALL').

Stations	PWRF ALL	PWRF EXTRA/%	PWRF STRONG	PWRF EXTEND	PWRF OTHER	PWRF NEW/%
Explorers Cove	13.0	**12.3/95**	4.8	5.3	4.5	**0.4/3**
Lake Fryxell	38.8	**26.2/68**	11.0	7.8	10.0	**2.2/6**
Lake Hoare	87.3	**65.0/74**	21.0	34.4	18.0	**8.8/10**
Lake Bonney	74.1	**46.6/63**	18.0	21.8	9.6	**9.6/13**
Taylor Glacier	121.5	**76.0/63**	37.2	45.4	2.2	**20.4/17**
Lake Brownworth	52.4	**36.2/69**	11.2	15.4	13.6	**2.8/5**
Lake Vanda	80.6	**48.2/60**	24.4	31.2	3.6	**8.4/10**
Lake Vida	33.3	**21.2/64**	9.4	9.8	5.8	**2.4 / 7**

more events than observed. We next categorize several types of missed events, shown in the next three columns and described below, that are then subtracted from this total.

'PWRF STRONG' represents observations that suggest a foehn event, but are too weak to meet the identification criteria. To identify these events, all of the criteria thresholds for observations are halved (except for wind direction), and the number of the LTER periods that switch from non-foehn to foehn with this weaker set of observed criteria is recorded. Visual inspection of the LTER and Polar WRF time series shows that Polar WRF is either premature with event initiation, or extends events too long (not shown). The values in column 'PWRF EXTEND' are obtained when an observed foehn event occurs within 24 h before or after an event that only occurs in Polar WRF. Finally, if there is an observed event at another station at the same time, meaning foehn is present over the MDVs but Polar WRF does not resolve it at a particular site, then 'PWRF OTHER' is iterated. When we subtract these three types of missed events (while accounting for overlap between categories), the new quantity of average missed events per summer is shown in column 'PWRF NEW' of Table 2. At all stations, there is a substantial reduction in the number of missed events, with all sites well under 20% of the total number of simulated events. Discrepancies between Polar WRF and the LTER observations are functions of the foehn criteria and are exacerbated by a positive wind speed bias over valleys in Polar WRF (e.g. Jiménez *et al.*, 2010). As shown in Table 2, the foehn events occurring only in Polar WRF according to the criteria are also present in the observations, but foehn events in Polar WRF are either stronger (PWRF STRONG), start early or last too long (PWRF EXTEND), or are misplaced spatially (PWRF OTHER).

Figure 4(b) shows the number of missed criteria for observed events that Polar WRF does not identify. At more western sites (Taylor Glacier, Lake Bonney, Lake Hoare, Lake Vanda, and Lake Vida), temperature and wind speed have the largest counts. At the eastern sites (Lake Brownworth, Lake Fryxell, and Explorers Cove), wind speed and wind direction have the largest totals. Table 3 shows the average number of observed events ('LTER ALL'), and the average number of missed events per summer that Polar WRF does not capture and the percentage of the total ('LTER EXTRA'). Discrepancies are more modest than for the extra events in Table 2 – most sites are under 50%. The 'LTER ABOVE 0' column shows the average number of the LTER-only events where the temperature criterion is met through the 0 °C threshold (i.e. Polar WRF is too cold). The 'LTER WEAK WIND' column shows the LTER events where the only missing criterion in Polar WRF is wind speed. When these events are removed, the new average number of events that Polar WRF misses per year is shown in the 'LTER NEW' column. Missed events are now generally below 25% of the total observed events. Events that Polar WRF misses are due to either the model cold bias, or misplaced localized features such as hydraulic jumps that can cause instances of underestimated wind speeds during foehn events (Steinhoff *et al.*, 2008; S13).

In summary, Polar WRF has too many foehn events compared with the LTER observations, and the number of extra Polar WRF events exceeds the number of events that the model misses. Polar WRF generally represents the interannual and spatial variability of foehn events in the MDVs, but extra foehn events in Polar WRF result from a positive wind-speed bias and foehn conditions lasting for too long and being too widespread. The source of the wind speed bias is not clear, but the incorrect foehn timing primarily results from the method of horizontal diffusion used in these Polar WRF simulations. For numerical stability reasons, horizontal diffusion is calculated on model vertical levels, whereas for the simulations in S13, accommodations were made for diffusion to be calculated in physical space, and foehn event timing errors were largely eliminated. Zängl *et al.* (2004a, 2004b) performed sensitivity experiments with horizontal diffusion options in MM5, and found that calculating diffusion on model surfaces lead to incorrect timing of foehn initiation in Alpine valleys. These errors dominated effects from horizontal

© 2013 Royal Meteorological Society

Table 3. Extra foehn events in the LTER observations compared with Polar WRF. 'LTER ALL' is the average number of observed foehn events each summer; 'LTER EXTRA' is the average number of foehn events in the LTER observations not found in Polar WRF each summer (and percentage of 'LTER ALL'); 'LTER ABOVE 0' and 'LTER WEAK WIND' are average number of Polar WRF biases each summer (described in text); and 'LTER NEW' is the average number of missed events each summer when discrepancies in previous two columns and their overlap are accounted for (and percentage of 'LTER ALL').

Stations	LTER ALL	LTER EXTRA/%	LTER ABOVE 0	LTER WEAK WIND	LTER NEW/%
Explorers Cove	7.9	**4.5/57**	2.7	0.5	**1.3/16**
Lake Fryxell	19.7	**9.5/48**	4.1	1.5	**4.4/22**
Lake Hoare	34.1	**11.5/34**	4.5	4.8	**3.8/11**
Lake Bonney	53.5	**27.7/52**	15.0	7.4	**10.6/20**
Taylor Glacier	81.1	**38.4/47**	13.5	13.3	**17.5/22**
Lake Brownworth	24.1	**9.5/39**	2.1	1.5	**6.2/26**
Lake Vanda	59.1	**24.2/41**	16.4	14.8	**3.6/6**
Lake Vida	22.9	**10.8/47**	7.0	5.4	**1.9/8**

model resolution. Observed events that Polar WRF misses result primarily from a model cold bias during foehn events.

4. Robustness of foehn mechanism

In S13, prominent mesoscale features were illustrated for an MDVs foehn case study from 29 December 2006 to 1 January 2007, which occurred at all the MDVs LTER sites. Here, we show the robustness of these features across other foehn events. The foehn criteria described in section 2.3 are used on the LTER AWS data to produce a set of 979 summer foehn events that occur at two or more sites over the 1994–2009 study period. This set corresponds to 'LTER ALL' of Table 3. Hence, we are using Polar WRF output corresponding to observed events. Even though there are some foehn events in observations not identified in the model, the analysis in the previous section showed that Polar WRF is primarily missing the local response at specific sites, and not the large-scale conditions leading to foehn. The interannual variability of the matched Polar WRF-LTER foehn events ('BOTH' in Figure 3) agrees well with that for the full set of the LTER foehn events (not shown).

4.1. *Gap flow*

Steinhoff *et al.* (2013) showed that foehn events are initiated by southerly gap flow over the western portion of the MDVs. The gap flow, extending vertically to the surrounding ridge height (between the higher elevation East Antarctic ice sheet to the west and the Royal Society Range to the east), is forced by the pressure difference along an elevated gap in the terrain south of the MDVs. The pressure difference along the gap is larger for easterly ambient flow, due to flow being blocked against the Transantarctic Mountains and higher pressure upstream of the gap, than for westerly ambient flow. Therefore, gap flow is more important in setting up southerly flow into the MDVs for easterly than westerly ambient flow. To determine if gap flow is stronger for easterly ambient flow across all identified foehn events, a scatter plot of the Polar WRF adjusted pressure difference along the gap against wind speed within the gap is presented in Figure 5. Pressure is adjusted to a constant height, defined here to be the highest point along the transect. The along-gap transect for the pressure difference and the averaging box for the wind speed are shown in Figure 2(b) (transect AA' and Box 1). In Figure 5, the data are colour-coded by 600 hPa wind direction and wind speed upstream (south) of the MDVs (600 hPa is the closest standard level above the transect, and 'upstream' refers to all points below the dashed line at $y = 50$ in Figure 2(b)). The purple points, representing weak ambient forcing, are clustered in the lower left corner of the plot, with weak gap wind speeds (generally less than 10 m s^{-1}) and weak gap forcing (along-gap adjusted pressure differences generally less than 2 hPa). Understandably, as the gap wind speed increases, more red (southeasterly forcing) and green (southwesterly forcing) points are found. The red points feature a stronger relationship between gap pressure difference and gap

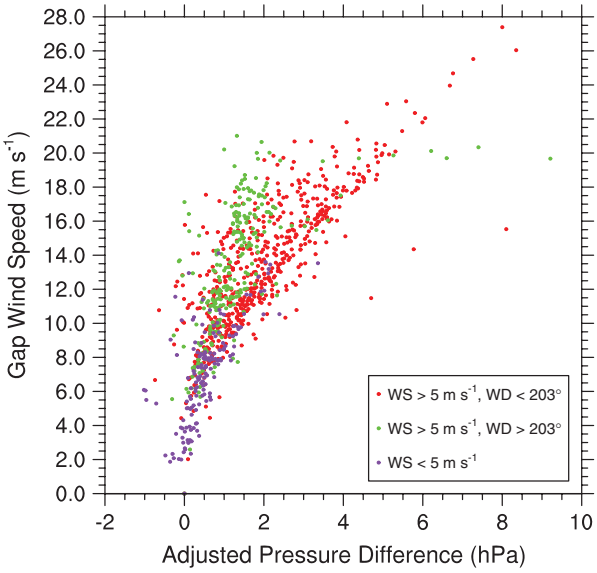

Figure 5. Scatter plot of Polar WRF along-gap adjusted pressure difference (hPa) versus near-surface gap wind speed (m s^{-1}). Values colour-coded according to 600 hPa wind speed (WS) and wind direction (WD) (see inset). Along-gap transect shown by AA' in Figure 2(b), near-surface gap wind speed averaged across Box 1 in Figure 2(b), and 600 hPa wind speed and wind direction averaged below $y = 50$ in Figure 2(b).

wind speed. As along-gap pressure difference increases, the gap wind speed increases. This relationship is weaker for the green points, where along-gap pressure differences remain relatively weak (less than 3 hPa), even for wind speeds approaching 20 m s^{-1}.

Flow-blocking south of the Royal Society Range and the ambient synoptic-scale pressure gradient are primarily responsible for the along-gap pressure difference, which drives the southerly gap flow into the western MDVs, even when the ambient wind direction is oblique to the gap axis. Figure 5 shows that the along-gap pressure difference is larger for easterly ambient flow, resulting in a stronger gap flow. In contrast, as ambient winds become westerly, flow blocking is greatly reduced because flow originates at a higher elevation over the East Antarctic ice sheet, and gap flow is less essential for foehn (S13).

4.2. *Mountain waves*

Mountain waves form over the complex terrain south of the MDVs, forced by gap flow when ambient flow does not have a westerly component (S13). For the case study presented in S13, the foehn characteristics changed with the direction and speed of the ambient wind south of the MDVs. The mountain wave response south of the MDVs depended on the non-dimensional mountain height, also known as the inverse Froude number,

$$M = \frac{Nh_m}{U}, \tag{1}$$

© 2013 Royal Meteorological Society

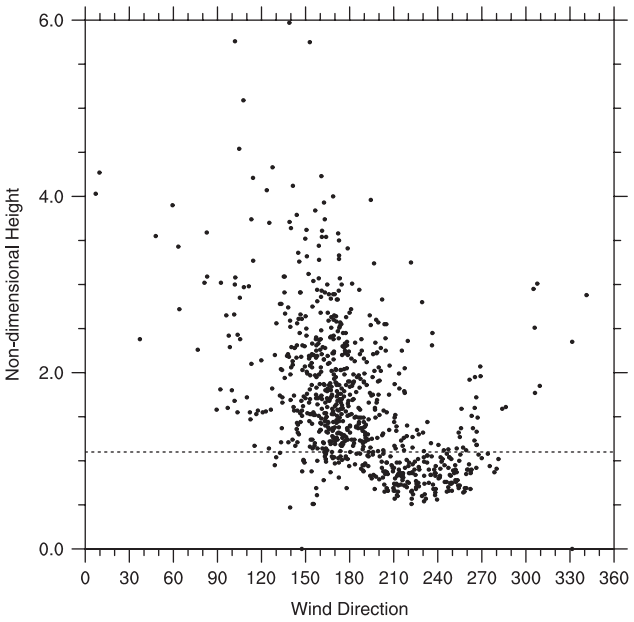

Figure 6. Scatter plot of Polar WRF 600 hPa wind direction (degrees) versus non-dimensional mountain height for all observed foehn events at two or more sites. Averaging area for non-dimensional mountain height represented by Box 2 in Figure 2(b), and 600 hPa wind direction averaged below $y = 50$ line in Figure 2(b). Dashed line represents non-dimensional mountain height of 1.1.

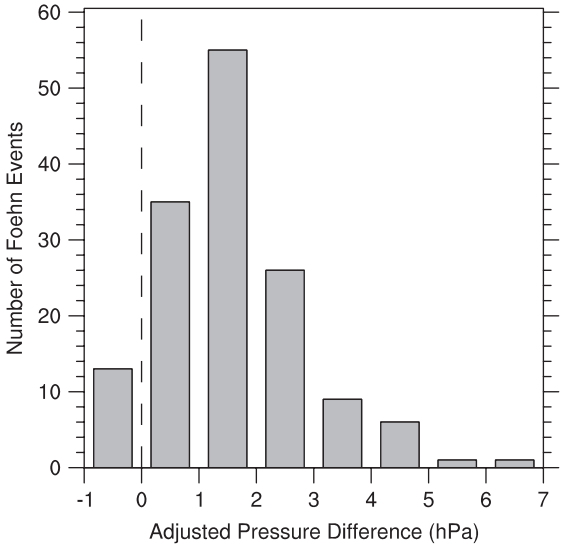

Figure 7. Histogram of Polar WRF adjusted pressure difference (hPa) along Taylor Valley between the two red points in Figure 2(b) for 146 foehn events recorded at Lake Fryxell and one other site. Positive values represent larger adjusted pressure in Taylor Valley than offshore.

where U is the mean-state layer-average wind speed, N is the mean-state Brunt–Väisälä frequency, and $h_m$is an estimate of the effective mountain height (the difference in height between the gap (Box 1 in Figure 2(b)) and the area upstream (Box 2 in Figure 2(b)), approximately 850 m). Southerly flow was blocked well south of the MDVs region, resulting in lower wind speeds and a larger non-dimensional mountain height. This lead to low-level wave breaking and hydraulic jumps south of Taylor Valley. When the ambient wind direction shifted more westerly, the non-dimensional mountain height decreased, wave breaking was not as pronounced, and observed wind speeds at the LTER AWS sites were higher.

To see if this relationship between wind direction south of the MDVs and the non-dimensional mountain height holds for more cases, a scatter plot of wind direction south of the MDVs (using Box 2 in Figure 2(b)) versus non-dimensional mountain height is plotted in Figure 6. A theoretical non-dimensional mountain height threshold of 1.1 separates linear flow at lower values from nonlinear flow with wave breaking at higher values (Smith and Grønås, 1993). In Figure 6, a large range in non-dimensional mountain height occurs for easterly wind directions. There is some difficulty in defining the non-dimensional mountain height for easterly ambient flow because it is blocked, yet a strong along-gap pressure difference leads to acceleration into the gap itself. Thus, for these wind directions, the along-gap pressure difference might be a better indicator of flow response over the gap, as discussed in section 4.1.

For southerly flow (wind direction from 180° to 205°), non-dimensional mountain heights generally remain above 1.1, indicating nonlinear flow and wave breaking, as was found for the case study. However, with wind directions greater than about 205°, nondimensional mountain heights decrease, with most values now under 1.1. This again agrees with the case study, where a westerly offshore wind is not blocked and results in vertically propagating mountain waves downstream of the gap.

4.3. *Pressure-driven channelling*

Mountain waves reach the western MDVs, directly resulting in foehn effects. While eastern MDVs sites do not often experience direct mountain wave effects, foehn effects still reach these locations. Pressure-driven channelling (e.g. Whiteman and Doran, 1993; McGowan *et al.*, 2002) is the mechanism responsible for the westerly flow that advects warm foehn air downvalley, as flow is forced by the component of the pressure gradient along the valley axis. The pressure gradient, represented by higher pressure over the western MDVs, is established by the pressure drag of mountain waves over the western MDVs, and weak flow offshore over McMurdo Sound. Conversely, foehn conditions can be interrupted by cool, moist easterly flow at eastern MDVs sites (i.e. *easterly intrusions*) when an opposing pressure gradient is directed onshore (S13). Here we focus on the forcing for westerly downvalley flow, showing that pressure-driven channelling is robust across a set of foehn events affecting the eastern MDVs.

Figure 7 shows the distribution of Polar WRF adjusted pressure differences between two points, one over western Taylor Valley and one offshore (red points in Figure 2(b)), for a set of 146 foehn events observed at multiple sites including Lake Fryxell. Lake Fryxell is chosen because it rarely experiences direct foehn effects (from mountain waves) due to blocking by the Royal Society Range (S13). Positive values represent higher adjusted pressure over western Taylor Valley. A clear majority (133 of 146) of these foehn events feature a downvalley-directed pressure gradient force, meaning that the flow of foehn air is directed downvalley towards the coast. Most of the events have a pressure difference of 0–3 hPa, similar in magnitude to the values found by S13. Therefore, the pressure-driven channelling mechanism proposed by S13 is robust across a set of foehn events that affect eastern Taylor Valley; the 13 events that feature a weak upvalley pressure gradient may be complicated by localized effects from mountain waves or terrain-induced circulations offshore.

5. Aspects of the large-scale circulation

5.1. *Synoptic-scale flow during extreme warming*

In S13, temperature changes during the foehn event, independent of diurnal effects, were attributed to differences in advection patterns aloft. The warmest period in the case study corresponds to an intrusion of warm, moist maritime air over Antarctica, which is brought to the surface in the MDVs by the foehn mechanism. Here we discuss the synoptic-scale patterns associated with the warmest foehn events.

Although Figure 6 shows that foehn events can occur through a wide range of wind directions, the events are not all independent, as most groupings of events occur consecutively. Of the 979 total observed foehn events considered, 498 of them (51%) are

© 2013 Royal Meteorological Society

part of an 'extended' foehn event, where the considered event is embedded in five straight days of foehn conditions in the MDVs. Foehn events are not scattered randomly across a season, but instead occur in 'outbreaks' associated with organized synoptic-scale patterns. Enhanced meridional flow, leading to intrusions of warm, moist air into East Antarctica, are often associated with blocking highs south of Australia and New Zealand (Bromwich *et al.*, 1993; Murphy and Simmonds, 1993; Goodwin *et al.*, 2003; Massom *et al.*, 2004; Fujita and Abe, 2006; Scarchilli *et al.*, 2011). To determine if the warmest foehn events are related to blocking, we compute a blocking index at various longitudes for the 73 warmest events (those that exceed 3 °C) at Lake Hoare from ERA-Interim. Lake Hoare is chosen because it is centrally located in Taylor Valley, and also has a reliable and long observation record. The blocking index (BI) used is that of Wright (1994), defined as

$$BI = 0.5(U_{25} + U_{30} + U_{55} + U_{60} - U_{40} - U_{50} - 2U_{45}), \quad (2)$$

where U is the zonal wind component at 500 hPa, subscripts indicate Southern Hemisphere latitudes, and BI is calculated along each longitude of interest. Positive values indicate a weak zonal component in midlatitudes, indicative of blocking. Although more sophisticated blocking indices exist (e.g. Wiedenmann *et al.*, 2002), an instantaneous blocking index is sufficient because we are not concerned about the duration of enhanced meridional flow. Positive blocking values for all of the warm events at longitudes ranging from 90°E to 90°W every 15° are shown in Figure 8(a). Blocking events are most common and strongest between 165°E and 150°W, just west of the southwest Pacific climatological maximum identified in previous studies (e.g. Sinclair, 1996; Renwick, 1998, 2005). The southeast Pacific climatological blocking region near 120°W is also represented in Figure 8(a). Fifty-one of the 73 warmest events feature a blocking index greater than 20.0 within the sector shown in Figure 8(a), where climatological average blocking index values are less than 3.0, suggesting that an amplified circulation pattern is responsible for warm air advection during foehn.

The 600 hPa vector winds are averaged along a transect from 90°E to 90°W between 70°S and 80°S, which is shown in Figure 8(b). A wave-2 pattern of meridional winds exists along the transect, with alternating northerly and southerly winds, and phase lines tilting eastward to the north. This pattern suggests high pressure over East Antarctica near 135°E, low pressure near 180°, and high pressure near 135°W. This is an amplified circulation pattern over Antarctica, which differs markedly from 'typical' Antarctic circulation patterns of storm systems circling the continent and Antarctica itself being isolated from the rest of the Southern Hemisphere. There is a southerly wind component southsouthwest of the MDVs, with maritime origin from the northerly flow between longitudes of 180° and 150°W (Figure 8(b)). Therefore, maritime intrusions appear to be responsible for warm events in the MDVs, as over the rest of the continent.

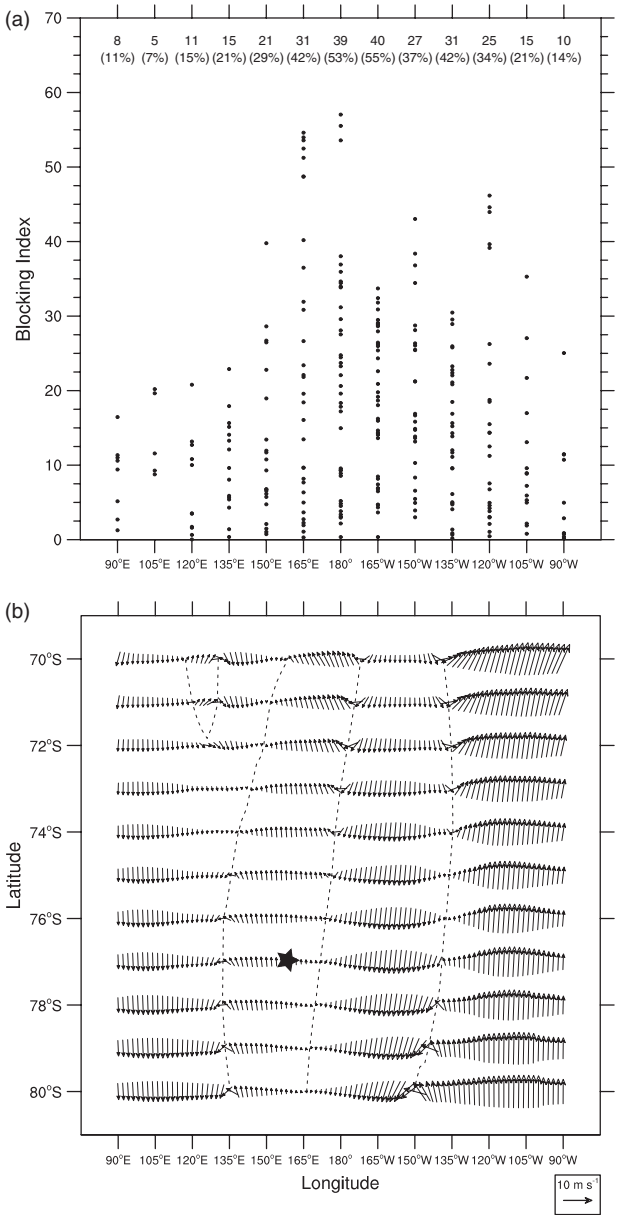

Figure 8. (a) Scatterplot of positive 500 hPa blocking indices from ERA-Interim for the 73 warmest foehn events at Lake Hoare (those with maximum observed temperature> +3 °C) according to the blocking index of Wright (1994) at longitudes indicated on the *x*-axis. Numbers at the top of the plot correspond to the number of events with positive blocking index values at this longitude, and the percentage of the 73 total events. (b) Average 600 hPa wind vectors for all 73 warmest foehn events at Lake Hoare. Dashed lines represent zero contour lines of average meridional wind. A reference vector is shown at the lower right and the star shows approximate location of MDVs.

5.2. *The role of intraseasonal variability – an example from summer 2001/2002*

Austral summer 2001/2002 was one of the warmest summers on record in the MDVs (Speirs *et al.*, 2013), and resulted in anomalously large melt and stream flow in the MDVs (Doran *et al.*, 2008; Hoffman *et al.*, 2008). Monthly temperature anomalies at Lake Hoare from November 2001 to February 2002 were −0.50, +1.50, +1.36, and +1.13 °C, respectively. Gamble (2003) provides a climatic summary of the season. Near-neutral ENSO conditions (indicated by the Southern Oscillation Index (SOI)) persisted from earlier in 2001, while in December 2001 an outgoing longwave radiation (OLR) index centred over the western tropical Pacific was in its most negative phase since October 1997, associated with an active Madden–Julian Oscillation (MJO) period. Additionally, an anomalously strong blocking index (Eq. (2)) was found at almost all longitudes in the Australia–New Zealand sector of the south Pacific, strongest in January and February 2002. As discussed by Massom *et al.* (2006), this season featured a positive SAM index throughout. Both Turner *et al.* (2002) and Massom *et al.* (2006) note the strong circumpolar trough and enhanced wavenumber-3/4 pattern of high pressure over the midlatitudes this season. The latter feature brought warm-air intrusions over the continent (Turner *et al.*, 2002; Massom *et al.*, 2004). These conditions are apparent from the 500 hPa geopotential height anomalies for November 2001–February 2002, compared with the corresponding period from 1979 to 2012 from ERA-Interim in Figure 9(a). Geopotential heights are lower around Antarctica, especially in the region of the Amundsen Sea low, and an enhanced wavenumber-3/4 pattern is seen in midlatitude positive anomalies.

The MDVs foehn events are sporadic and clustered together in time, suggesting that there is considerable intraseasonal

© 2013 Royal Meteorological Society

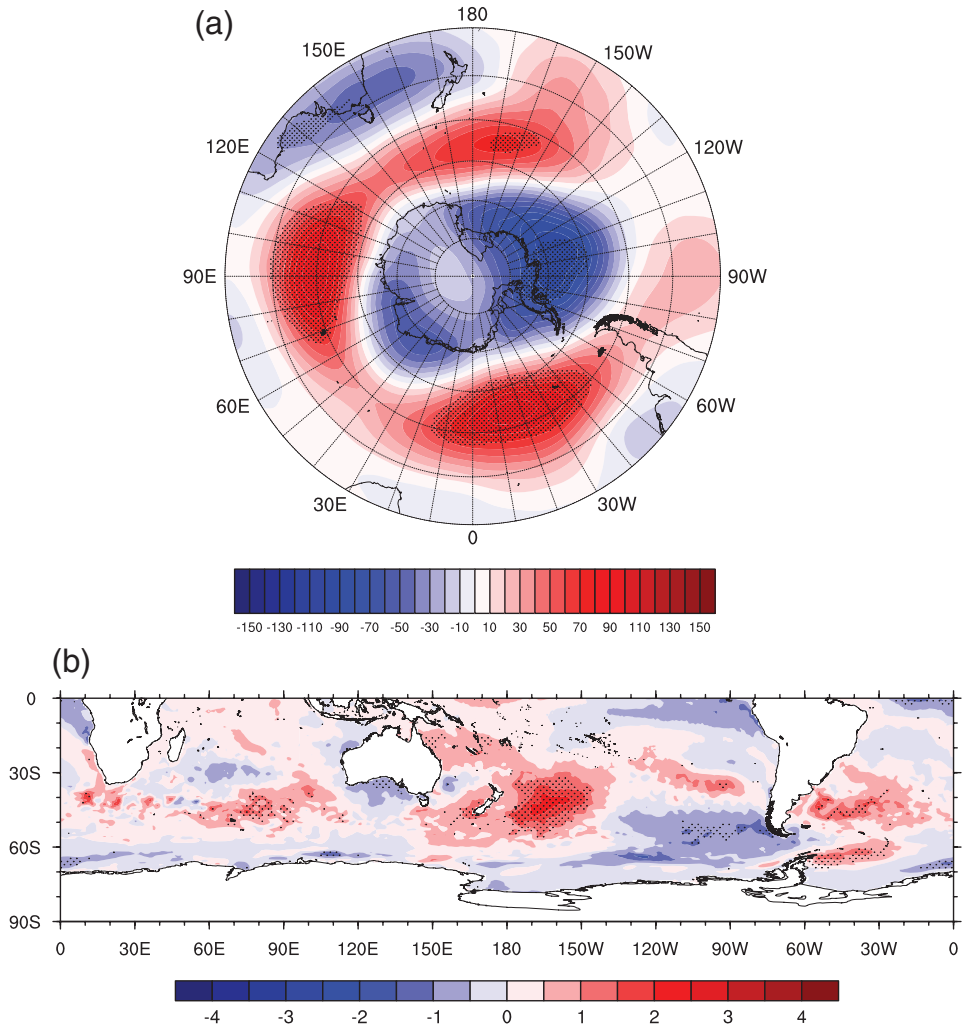

Figure 9. ERA-Interim NDJF 2001/2002 anomalies, relative to the 1979–2012 period, for (a) 500 hPa geopotential height (m) and (b) sea-surface temperature (K). Stippled areas represent anomalies of magnitude greater than two standard deviations.

variability associated with their occurrence. There are 23 six-hourly periods of foehn conditions with temperature greater than 3 °C at Lake Hoare during the 2001/2002 austral summer season, occurring on only 11 days, and during only three distinct time periods. The ERA-Interim and Polar WRF 500 hPa geopotential height fields are shown for the prominent 10–12 January 2002 foehn event, when the temperature exceeded 9 °C at Lake Hoare, in Figure 10. A pronounced blocking high is positioned southwest of New Zealand, with poleward flow extending from southeast Australia to interior East Antarctica. A massive cyclonic circulation exists over the western hemisphere sector. Near-record high temperatures were recorded at Vostok (East Antarctica) and South Pole during this time period (Massom *et al.*, 2004). This example is representative of two other extended foehn events over the 2001/2002 austral summer that brought anomalously warm conditions to the MDVs.

Beyond ENSO and SAM, a possible explanation for the warm conditions is the South Pacific Wave (SPW). This is the fourth EOF of geopotential height or streamfunction interannual variability, as discussed by Kiladis and Mo (1998), Kidson (1999) and Frederiksen and Zheng (2007). The SPW is associated with a wavetrain source over northern Australia (Frederiksen and Zheng, 2007). The geopotential height anomaly pattern in Figure 9(a) is similar to the fourth slowly varying EOF in Frederiksen and Zheng (2007). Furthermore, the pattern of SST anomalies in Figure 9(b) corresponds with the one-point DJF SST-EOF4 correlations in Frederiksen and Zheng (2007, their figure 5d), in particular the meridional dipole in the southern Indian Ocean, negative anomalies south of Australia, and positive anomalies south and east of New Zealand.

6. Discussion

Studies of intraseasonal variability show the dominance of wavenumber 4–5 patterns in Southern Hemisphere mid- and high latitudes during summer (e.g. Kiladis and Mo, 1998; Kidson, 1999; Frederiksen and Zheng, 2007). While atmospheric blocking events have been attributed to interannual variability, particularly with ENSO (e.g. Renwick, 1998; Kidson *et al.*, 2002), blocking has also been linked to intraseasonal variability (Frederiksen and Frederiksen, 1993; Mo and Higgins, 1998; Renwick and Revell, 1999; Frederiksen and Zheng, 2007). Massom *et al.* (2004) analyze three case studies of enhanced precipitation and warm conditions over interior East Antarctica (one of which includes austral summer 2001/2002). In all three cases, a blocking high southwest of New Zealand is a prominent feature, and just a few blocking episodes can deliver a significant portion of mean annual precipitation. In section 5.2 the SPW (EOF4) signal was implicated for the extraordinary austral summer 2001/2002 season. This signal probably reflects strong intraseasonal variability that affects the southwest Pacific (Mo and Higgins, 1998; Kidson, 1999; Renwick, 2005; Hobbs and Raphael, 2010). Furthermore, associations between ENSO and blocking are weaker in the southwest Pacific, the main sector of blocking associated with MDVs foehn, than for the southeast Pacific (Renwick, 2005).

Although the extended foehn events of austral summer 2001/2002 featured similar synoptic-scale patterns leading to blocking in the southwest Pacific, varied circulation patterns can produce strong pressure/height gradients over the MDVs leading to foehn. This is illustrated by the wide range of ambient wind directions that can lead to foehn generation, and is also clear from a perusal of 500 hPa geopotential height maps during

© 2013 Royal Meteorological Society

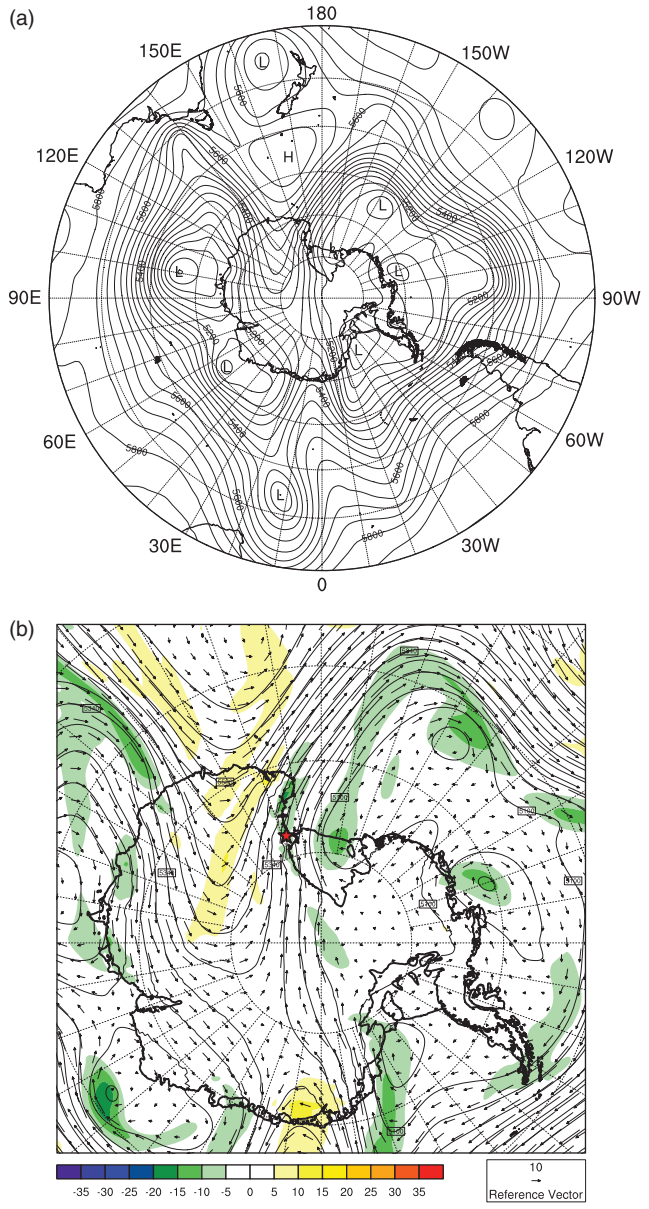

Figure 10. The 500 hPa geopotential height (contours, m) at 0000 UTC 11 January 2002 from (a) ERA-Interim and (b) Polar WRF. The latter also contains relative vorticity (10^{-5} s^{-1}, colour shaded) and wind vectors and a red star representing the approximate location of the MDVs.

foehn events. For example, a foehn event outbreak in November 1997 was associated with an El Niño-related pattern of increased geopotential heights across Antarctica and decreased heights south of New Zealand, setting up anomalously strong easterly flow over the MDVs. In contrast, a warm period in late January 1996, with weak positive SAM conditions (SAM index value of +0.55) but moderate La Niña conditions (SOI of +1.6), features an anomalously strong Amundsen Sea low (known to be associated with La Niña forcing (Kwok and Comiso, 2002)) that advects warm maritime air across West Antarctica, consistent with the hypothesis of Bertler *et al.* (2004). Thus, the MDVs foehn events can occur with a wide variety of synoptic-scale patterns and modes of large-scale variability, since the primary factor inducing foehn events is strong ambient flow aloft. Similarly, it is difficult to definitively attribute Antarctic intraseasonal variability to tropical forcing (Renwick *et al.*, 2012), and we are unable to find statistically significant correlations between the MJO and foehn events over the study period.

7. Conclusions

The foehn mechanism proposed by S13 for the MDVs has been shown to be robust across a set of summer foehn events over the 1994–2009 period. Gap flow brings southerly flow into the southern MDVs, evidenced by the positive relationship between the adjusted pressure difference along the gap and near-surface wind speed, especially for ambient flow with an easterly component. Mountain waves form over the complex terrain south of the MDVs, leading to adiabatic warming and the foehn effect, and the non-dimensional mountain height, indicative of flow linearity, is dependent on the ambient wind direction. Nonlinearity is more prevalent for southerly ambient flow, leading to weaker MDVs foehn events. These effects decrease when ambient flow becomes more westerly, and foehn events are stronger. Pressure-driven channelling then brings the warm air downvalley, and this effect is robust across the set of foehn events examined. These results reinforce the case made by Speirs *et al.* (2010) and S13 that strong wind and warming events in the MDVs result from a foehn effect, and not a katabatic effect, as had been inferred in previous studies.

Speirs *et al.* (2010) found that an increase in foehn events in 2007 over 2006 resulted from an increased synoptic-scale pressure gradient over the MDVs, resulting primarily from increased sea-level pressure over the Southern Ocean south of Australia. This feature is confirmed for a longer study period to be prevalent for the warmest foehn events, associated with atmospheric blocking in the Australian sector. Still, foehn winds can occur over a wide range of ambient wind directions, and there are no specific synoptic-scale patterns responsible for foehn events. The variety of synoptic-scale patterns resulting in foehn events perhaps explains the tenuous connections between modes of interannual variability (e.g. SAM and ENSO) and MDVs foehn and warm events (Bertler *et al.*, 2004; Speirs *et al.*, 2013). While a maritime influence is indeed responsible for the warmest foehn events (Bertler *et al.*, 2004), a simple ENSO-related shift in atmospheric circulation over West Antarctica and the Ross Ice Shelf cannot explain MDVs summer temperature variability. Furthermore, the foehn effect is necessary to bring the maritime air to the surface over the MDVs.

The episodic nature of MDVs foehn events suggests the importance of intraseasonal variability. Further research on MDVs and Antarctic-wide warm-air and moisture intrusions should focus on intraseasonal variability, of which the tropical connections to and the internal generation of such events are not well understood.

Acknowledgements

This research is supported by the National Science Foundation via NSF Grant ANT-0636523. High-performance computing support is provided by NCAR's Computational and Information Systems Laboratory, sponsored by the National Science Foundation, and the Ohio Supercomputing Center. The McMurdo Dry Valleys LTER Program provided automatic weather station data. Kevin Manning provided the bare-ground land-use data for the MDVs. NCAR is sponsored by the National Science Foundation and other agencies.

References

Bertler NAN, Barrett PJ, Mayewski PA, Fogt RL, Kreutz KJ, Shulmeister J. 2004. El Niño suppresses Antarctic warming. *Geophys. Res. Lett.* **31**: L15207, doi: 10.1029/2004GL020749.

Bertler NAN, Naish TR, Oerter H, Kipfstuhl S, Barrett PJ, Mayewski PA, Kreutz K. 2006. The effects of joint ENSO–Antarctic Oscillation forcing on the McMurdo Dry Valleys, Antarctica. *Antarct. Sci.* **18**: 507–514.

Bromley AM. 1985. *Weather Observations, Wright Valley, Antarctica*, Information Publication 11. New Zealand Meteorological Service: Wellington, New Zealand.

Bromwich DH, Carrasco JF, Liu Z, Tzeng RT. 1993. Hemispheric atmospheric variations and oceanographic impacts associated with katabatic surges across the Ross ice shelf, Antarctica. *J. Geophys. Res.* **98**: 13045–13062, doi: 10.1029/93JD00562.

Bromwich DH, Monaghan AJ, Guo Z. 2004. Modeling the ENSO modulation of Antarctic climate in the late 1990s with the Polar MM5. *J. Clim.* **17**: 109–132.

© 2013 Royal Meteorological Society

Bromwich DH, Hines KM, Bai LS. 2009. Development and testing of Polar Weather Research and Forecasting model: 2. Arctic Ocean. *J. Geophys. Res.* **114**: D08122, doi: 10.1029/2008JD010300.
Bromwich DH, Otieno FO, Hines KM, Manning KW, Shilo E. 2013. A comprehensive evaluation of Polar WRF forecast performance in the Antarctic. *J. Geophys. Res.* **118**: 274–292, doi: 10.1029/2012JD018139.
Campbell IB, Claridge GGC, Campbell DI, Balks MR. 1998. The soil environment of the McMurdo Dry Valleys, Antarctica. *Ecosystem Dynamics in a Polar Desert, the McMurdo Dry Valleys, Antarctica*, Priscu JC. (ed.) *Antarctic Research Series* **72**: 297–322. American Geophysical Union: Washington, DC.
Carleton AM. 2003. Atmospheric teleconnections involving the Southern Ocean. *J. Geophys. Res.* **108**: 8080, doi: 10.1029/2000JC000379.
Carvalho LMV, Jones C, Ambrizzi T. 2005. Opposite phases of the Antarctic Oscillation and relationships with intraseasonal to interannual activity in the tropics during the austral summer. *J. Clim.* **18**: 702–718.
Chen F, Dudhia J. 2001. Coupling an advanced land surface-hydrology model with the Penn State-NCAR MM5 modeling system. Part I: Model implementation and sensitivity. *Mon. Weather Rev.* **129**: 569–585.
Comiso J. 1999. *Bootstrap Sea Ice Concentrations from NIMBUS-7 SMMR and DMSP SMM/I, 1989–2008.* National Snow and Ice Data Center, Digital Media: Boulder, CO.
Dee DP, Uppala SM, Simmons AJ, Berrisford P, Poli P, Kobayashi S, Andrae U, Balmaseda MA, Balsamo G, Bauer P, Bechtold P, Beljaars ACM, van de Berg L, Bidlot J, Bormann N, Delsol C, Dragani R, Fuentes M, Geer AJ, Haimberger L, Healy SB, Hersbach H, Hólm EV, Isaksen L, Kållberg P, Köhler M, Matricardi M, McNally AP, Monge-Sanz BM, Morcrette JJ, Park BK, Peubey C, de Rosnay P, Tavolato C, Thépaut JN, Vitart F. 2011. The ERA-Interim reanalysis: Configuration and performance of the data assimilation system. *Q. J. R. Meteorol. Soc.* **137**: 553–597.
Ding Q, Steig EJ, Battisti DS, Wallace JM. 2012. Influence of the tropics on the Southern Annular Mode. *J. Clim.* **25**: 6330–6348.
Doran PT, Dana GL, Hastings JT, Wharton RA. 1995. McMurdo Dry Valleys Long-Term Ecological Research (LTER): LTER automatic weather network (LAWN). *Antarct. J. U.S.* **30**: 276–280.
Doran PT, McKay CP, Clow GD, Dana GL, Fountain AG, Nylen T, Lyons WB. 2002. Valley floor climate observations from the McMurdo Dry Valleys, Antarctica, 1986–2000. *J. Geophys. Res.* **107**: 4772, doi: 10,1029/2001JD002045.
Doran PT, McKay CP, Fountain AG, Nylen T, McKnight DM, Jaros C, Barrett JE. 2008. Hydrologic response to extreme warm and cold summers in the McMurdo Dry Valleys, East Antarctica. *Antarct. Sci.* **20**: 499–509.
Fogt RL, Bromwich DH. 2006. Decadal variability of the ENSO teleconnection to the high-latitude south Pacific governed by coupling with the southern annular mode. *J. Clim.* **19**: 979–997.
Fogt RL, Bromwich DH, Hines KM. 2011. Understanding the SAM influence on the south Pacific ENSO teleconnection. *Clim. Dyn.* **36**: 1555–1576, doi: 10.1007/s00382-010-0905-0.
Fountain AG, Lyons WB, Burkins MB, Dana GL, Doran PT, Lewis KJ, McKnight DM, Moorhead DL, Parsons AN, Priscu JC, Wall DH, Wharton RA, Virginia RA. 1999. Physical controls on the Taylor Valley ecosystem. *Bioscience* **49**: 961–971.
Fountain AG, Nylen TH, Monaghan AJ, Basagic AJ, Bromwich DH. 2010. Snow in the McMurdo Dry Valleys, Antarctica. *Int. J. Climatol.* **30**: 633–642.
Frederiksen JS, Frederiksen CS. 1993. Monsoon disturbances, intraseasonal oscillations, teleconnection patterns, blocking, and storm track of the global atmosphere during January 1979: Linear theory. *J. Atmos. Sci.* **50**: 1349–1372.
Frederiksen CS, Zheng X. 2007. Variability of seasonal-mean fields arising from intraseasonal variability. Part 3: Application to SH winter and summer circulations. *Clim. Dyn.* **28**: 849–866.
Fujita K, Abe O. 2006. Stable isotopes in daily precipitation at Dome Fuji, East Antarctica. *Geophys. Res. Lett.* **33**: L18503, doi: 10.1029/2006GL026936.
Gamble FM. 2003. Seasonal climate summary southern hemisphere (summer 2001/02): A continuation of near-normal conditions in the tropical Pacific. *Aust. Meteorol. Mag.* **52**: 63–72.
Gong T, Feldstein SB, Luo D. 2010. The impact of ENSO on wave breaking and Southern Annular Mode events. *J. Atmos. Sci.* **67**: 2854–2870.
Goodwin I, de Angelis M, Pook M, Young NW. 2003. Snow accumulation variability in Wilkes Land, East Antarctica, and the relationship to atmospheric ridging in the 130°–170°E region since 1930. *J. Geophys. Res.* **108**: D21, doi: 10.1029/2002JD002995.
Gregory S, Noone D. 2008. Variability in the teleconnection between the El Niño-Southern Oscillation and West Antarctic climate deduced from West Antarctic ice core isotope records. *J. Geophys. Res.* **113**: D17110, doi: 10.1029/2007JD009107.
Guo Z, Bromwich DH, Hines KM. 2004. Modeled Antarctic precipitation. Part II: ENSO modulation over West Antarctica. *J. Clim.* **17**: 448–465.
Hines KM, Bromwich DH. 2008. Development and testing of Polar Weather Research and Forecasting (WRF) Model. Part I: Greenland ice sheet meteorology. *Mon. Weather Rev.* **136**: 1971–1989.
Hines KM, Bromwich DH, Bai LS, Barlage M, Slater AG. 2011. Development and testing of Polar WRF. Part III. Arctic land. *J. Clim.* **24**: 26–48, doi: 10.1175/2010JCLI3460.1.
Hobbs WR, Raphael MN. 2010. Characterizing the zonally asymmetric component of the SH circulation. *Clim. Dyn.* **35**: 859–873.
Hoffman MJ, Fountain AG, Liston GE. 2008. Surface energy balance and melt thresholds over 11 years at Taylor Glacier, Antarctica. *J. Geophys. Res.* **113**: F04014, doi: 10.1029/2008JF001029.
Hunt HW, Fountain AG, Doran PT, Basagic H. 2010. A dynamic physical model for soil temperature and water in Taylor Valley, Antarctica. *Antarct. Sci.* **22**: 419–434, doi: 10.1017/S0954102010000234.
Jiménez PA, Dudhia J. 2012. Improving the representation of resolved and unresolved topographic effects on surface wind in the WRF model. *J. Appl. Meteorol. Climatol.* **51**: 300–316.
Jiménez PA, González-Rouco JF, García-Bustamante E, Navarro J, Montávez JP, Vilà-Guerau de Arellano J, Dudhia J, Roldán A. 2010. Surface wind regionalization over complex terrain: Evaluation and analysis of a high-resolution WRF numerical simulation. *J. Appl. Meteorol. Climatol.* **49**: 268–287.
Karoly DJ. 1989. Southern Hemisphere circulation features associated with El Niño–Southern Oscillation events. *J. Clim.* **2**: 1239–1252.
Kidson JW. 1999. Principal modes of Southern Hemisphere low-frequency variability obtained from NCEP-NCAR reanalyses. *J. Clim.* **12**: 2808–2830.
Kidson JW, Revell MJ, Bhaskaran B, Mullan AB, Renwick JA. 2002. Convection patterns in the tropical Pacific and their influence on the atmospheric circulation at higher latitudes. *J. Clim.* **15**: 137–159.
Kiladis GN, Mo KC. 1998. Interannual and intraseasonal variability in the Southern Hemisphere. In *Meteorology of the Southern Hemisphere*, Karoly DJ, Vincent DG. (eds.) 307–336. American Meteorological Society: Boston, MA.
Kwok R, Comiso JC. 2002. Southern Ocean climate and sea ice anomalies associated with the Southern Oscillation. *J. Clim.* **15**: 487–501.
Lancaster N. 2004. Relations between aerodynamic and surface roughness in a hyper-arid cold desert: McMurdo Dry Valleys, Antarctica. *Earth Surf. Processes Landforms* **29**: 853–867.
L'Heureux ML, Thompson DWJ. 2006. Observed relationships between the El Niño–Southern Oscillation and the extratropical zonal-mean circulation. *J. Clim.* **19**: 276–287.
Liu H, Jezek K, Li B, Zhao Z. 2001. *Radarsat Antarctic Mapping Project Digital Elevation Model Version 2*. National Snow and Ice Data Center. Digital Media: Boulder, CO.
Massom RA, Pook MJ, Comiso JC, Adams N, Turner J, Lachlan-Cope T, Gibson TT. 2004. Precipitation over the interior East Antarctic ice sheet related to midlatitude blocking-high activity. *J. Clim.* **17**: 1914–1928.
Massom RA, Stammerjohn SE, Smith RC, Pook MJ, Iannuzzi RA, Adams N, Martinson DG, Vernet M, Fraser WR, Quetin LB, Ross RM, Massom Y, Krouse HR. 2006. Extreme anomalous atmospheric circulation in the West Antarctic peninsula region in austral spring and summer 2001/02, and its profound impact on sea ice and biota. *J. Clim.* **19**: 3544–3571.
McGowan HA, Sturman AP, Kossmann M, Zawar-Reza P. 2002. Observations of foehn onset in the Southern Alps, New Zealand. *Meteorol. Atmos. Phys.* **79**: 215–230.
McKendry IG, Lewthwaite EWD. 1992. Summertime along-valley wind variations in the Wright Valley Antarctica. *Int. J. Climatol.* **12**: 587–596.
Mo KC, Higgins RW. 1998. The Pacific–South American modes and tropical convection during the Southern Hemisphere winter. *Mon. Weather Rev.* **126**: 1581–1596.
Murphy BF, Simmonds I. 1993. An analysis of strong wind events simulated in a GCM near Casey in the Antarctic. *Mon. Weather Rev.* **121**: 522–534.
Northcott ML, Gooseff MN, Barrett JE, Zeglin LH, Takacs-Vesbach CD, Humphrey J. 2009. Hydrologic characteristics of lake- and stream-side riparian wetted margins in the McMurdo Dry Valleys, Antarctica. *Hydrol. Processes* **23**: 1255–1267.
Nylen TH, Fountain AG, Doran PT. 2004. Climatology of katabatic winds in the McMurdo Dry Valleys, Southern Victoria Land, Antarctica. *J. Geophys. Res.* **109**: D03114, doi: 10.1029/2003JD002927.
Pezza AB, Durrant T, Simmonds I. 2008. Southern Hemisphere synoptic behavior in extreme phases of SAM, ENSO, sea ice extent, and southern Australia rainfall. *J. Clim.* **21**: 5566–5584.
Pohl B, Fauchereau N, Reason CJC, Rouault M. 2010. Relationships between the Antarctic Oscillation, the Madden–Julian Oscillation, and ENSO, and consequences for rainfall analysis. *J. Clim.* **23**: 238–253, doi: 10.1175/2009JCLI2443.1.
Priscu JC, Fritsen CH, Adams EE, Giovannoni SJ, Paerl HW, McKay CP, Doran PT, Gordon DA, Lanoil BD, Pinckney JL. 1998. Perennial Antarctic lake ice: An oasis for life in a polar desert. *Science* **280**: 2095–2098.
Renwick JA. 1998. ENSO-related variability in the frequency of South Pacific blocking. *Mon. Weather Rev.* **126**: 3117–3123.
Renwick JA. 2005. Persistent positive anomalies in the Southern Hemisphere circulation. *Mon. Weather Rev.* **133**: 977–988.
Renwick JA, Revell MJ. 1999. Blocking over the South Pacific and Rossby wave propagation. *Mon. Weather Rev.* **127**: 2233–2247.
Renwick JA, Kohout A, Dean S. 2012. Atmospheric forcing of Antarctic sea ice on intraseasonal time scales. *J. Clim.* **25**: 5962–5975, doi: 10.1175/JCLI-D-11-00423.1.
Reynolds RW, Smith TM, Liu C, Chelton DB, Casey KS, Schlax MG. 2007. Daily high-resolution-blended analyses for sea surface temperature. *J. Clim.* **20**: 5473–5496.
Riordan AJ. 1975. The climate of Vanda Station, Antarctica. In *Climate of the Arctic*, Weller G, Bowling SA (eds.) 268–275. University of Alaska, Geophysical Institute: Fairbanks, AK.
Scarchilli C, Frezzotti M, Ruti PM. 2011. Snow precipitation at four ice core sites in East Antarctica: Provenance, seasonality and blocking factors. *Clim. Dyn.* **37**: 2107–2125, doi: 10.1007/s00382-010-0946-4.
Sinclair M. 1996. A climatology of anticyclones and blocking for the Southern Hemisphere. *Mon. Weather Rev.* **124**: 245–255.

© 2013 Royal Meteorological Society

Skamarock WC, Klemp JB, Dudhia J, Gill DO, Barker DM, Duda M, Huang XY, Wang W, Powers JG. 2008. 'A description of the advanced research WRF version 3', NCAR Tech Notes-475+STR. NCAR: Boulder, CO.
Smith RB, Grønås S. 1993. Stagnation points and bifurcation in 3-D mountain airflow. *Tellus* **45A**: 28–43.
Speirs JC, Steinhoff DF, McGowan HA, Bromwich DH, Monaghan AJ. 2010. Foehn winds in the McMurdo Dry Valleys, Antarctica: The origin of extreme warming events. *J. Clim.* **23**: 3577–3598.
Speirs JC, McGowan HA, Steinhoff DF, Bromwich DH. 2013. Regional climate variability driven by foehn winds, McMurdo Dry Valleys, Antarctica. *Int. J. Climatol.* **33**: 945–958, doi: 10.1002/joc.3481.
Spreen G, Kaleschke L, Heygster G. 2008. Sea ice remote sensing using AMSR-E 89 GHz channels. *J. Geophys. Res.* **113**: C02S03, doi: 10.1029/2005JC003384.
Stauffer DR, Seaman NL. 1994. Multiscale four-dimensional data assimilation. *J. Appl. Meteorol.* **33**: 416–434.
Steinhoff DF, Bromwich DH, Lambertson M, Knuth SL, Lazzara MA. 2008. A dynamical investigation of the May 2004 McMurdo Antarctica severe wind event using AMPS. *Mon. Weather Rev.* **136**: 7–26.
Steinhoff DF, Bromwich DH, Monaghan AJ. 2013. Dynamics of the foehn mechanism in the McMurdo Dry Valleys of Antarctica from Polar WRF. *Q. J. R. Meteorol. Soc.* **139**: 1615–1631, doi: 10.1002/qj.2038.
Thompson DWJ, Wallace JM. 2000. Annular modes in the extratropical circulation. Part I: Month-to-month variability. *J. Clim.* **13**: 1000–1016.
Thompson DC, Craig RMF, Bromley AM. 1971. Climate and surface heat balance in an Antarctic Dry Valley. *N. Z. J. Sci.* **14**: 245–251.
Turner J. 2004. Review: The El Niño-Southern Oscillation and Antarctica. *Int. J. Climatol.* **24**: 1–31.
Turner J, Harangozo SA, Marshall GJ, King JC, Colwell SR. 2002. Anomalous atmospheric circulation over the Weddell Sea, Antarctica during the austral summer of 2001/02 resulting in extreme sea ice conditions. *Geophys. Res. Lett.* **29**: 2160, doi: 10.1029/2002GL015565.
Whiteman CD, Doran JC. 1993. The relationship between overlying synoptic-scale flows and winds within a valley. *J. Appl. Meteorol.* **32**: 1669–1682.
Wiedenmann JM, Lupo AR, Mokhov II, Tikhonova EA. 2002. The climatology of blocking anticyclones for the northern and southern hemispheres: Block intensity as a diagnostic. *J. Clim.* **15**: 3459–3473.
Worby AP, Geiger CA, Paget MJ, Van Woert ML, Ackley SF, DeLiberty TL. 2008. Thickness distribution of Antarctic sea ice. *J. Geophys. Res.* **113**: C05S92, doi: 10.1029/2007JC004254.
Wright WJ. 1994. Seasonal climate summary southern hemisphere (autumn 1993): A second mature ENSO phase. *Aust. Meteorol. Mag.* **43**: 205–221.
Yu L, Zhang Z, Zhou M, Zhong S, Sun B, Hsu H, Gao Z, Wu H, Ban J. 2011. The intraseasonal variability of winter semester surface air temperature in Antarctica. *Polar Res.* **30**: 6039, doi: 10.3402/polar.v30i0.6039.
Yuan X. 2004. ENSO-related impacts on Antarctic sea ice: A synthesis of phenomenon and mechanisms. *Antarct. Sci.* **16**: 415–425.
Zängl G, Chimani B, H?berli C. 2004a. Numerical simulations of the foehn in the Rhine Valley on 24 October 1999 (MAP IOP 10). *Mon. Weather Rev.* **132**: 368–389.
Zängl G, Gohm A, Geier G. 2004b. South foehn in the Wipp Valley–Innsbruck region: Numerical simulations of the 24 October 1999 case (MAP-IOP 10). *Meteorol. Atmos. Phys.* **86**: 213–243.

© 2013 Royal Meteorological Society